Dual-basis reconstruction techniques for tomographic PIV

ARTICLE *in* SCIENCE CHINA TECHNOLOGICAL SCIENCES · AUGUST 2015

Impact Factor: 1.19 · DOI: 10.1007/s11431-015-5909-x

5 AUTHORS, INCLUDING:

Qi Gao
Beihang University(BUAA)
17 PUBLICATIONS **36** CITATIONS
SEE PROFILE

Wei Runjie
Amgen
10 PUBLICATIONS **41** CITATIONS
SEE PROFILE

Jinjun Wang
Beihang University(BUAA)
115 PUBLICATIONS **845** CITATIONS
SEE PROFILE

SCIENCE CHINA
Technological Sciences

• Article •

doi: 10.1007/s11431-015-5909-x

Dual-basis reconstruction techniques for tomographic PIV

YE ZhiJian[1], GAO Qi[1*], WANG HongPing[1], WEI RunJie[2] & WANG JinJun[1]

[1]*Fluid Mechanics Key Laboratory of Education Ministry, Beijing University of Aeronautics and Astronautics, Beijing 100191, China;*
[2]*MicroVec. Inc., Beijing 100083, China*

Received January 12, 2015; accepted June 25, 2015

As an inverse problem, particle reconstruction in tomographic particle image velocimetry attempts to solve a large-scale underdetermined linear system using an optimization technique. The most popular approach, the multiplicative algebraic reconstruction technique (MART), uses entropy as an objective function in the optimization. All available MART-based methods are focused on improving the efficiency and accuracy of particle reconstruction. However, those methods do not perform very well on dealing with ghost particles in highly seeded measurements. In this report, a new technique called dual-basis pursuit (DBP), which is based on the basis pursuit technique, is proposed for tomographic particle reconstruction. A template basis is introduced as *a priori* knowledge of a particle intensity distribution combined with a correcting basis to enable a full span of the solution space of the underdetermined linear system. A numerical assessment test with 2D synthetic images indicated that the DBP technique is superior to MART method, can completely recover a particle field when the number of particles per pixel (*ppp*) is less than 0.15, and can maintain a quality factor Q of above 0.8 for *ppp* up to 0.30. Unfortunately, the DBP method is difficult to utilize in 3D applications due to the cost of its excessive memory usage. Therefore, a dual-basis MART was designed that performed better than the traditional MART and can potentially be utilized for 3D applications.

tomographic PIV, particle reconstruction, dual-basis pursuit, multiplicative algebraic reconstruction technique

Citation: Ye Z J, Gao Q, Wang H P, et al. Dual-basis reconstruction techniques for tomographic PIV. Sci China Tech Sci, 2015, doi: 10.1007/s11431-015-5909-x

1 Introduction

Due to its outstanding performance of 3D three-component (3D3C) velocity measurements, tomographic particle image velocimetry (Tomo-PIV) has rapidly become a widely used and accurate approach of volumetric measurement method [1,2]. This technique mainly relies on the success of its particle reconstruction method, which obtains the 3D tracer distribution by analyzing 2D particle images that are simultaneously recorded on cameras (three or four, in general) at different viewing angles. The three-component velocity field in the measured volume can then be obtained by volumetric cross-correlation.

Iterative algebraic methods [3] are commonly used in tomographic reconstruction since they are simple and versatile and have the ability to handle under-sampled and large-scale data, even with noise [4]. The multiplicative algebraic reconstruction technique (MART) was first introduced into volumetric PIV by Elsinga et al. [1] and was originally proposed by Gordon et al. [5] for medical tomography. In mathematical terms, the MART attempts to solve the underdetermined system of equations using the theory of maximum entropy. This technique broadens the thoughts and promotes the development of volumetric velocity measurements. Atkinson and Soria [6] developed a simultaneous multiplicative algebraic reconstruction technique (SMART), which is characterized by significant improvements in computing time and memory usage without any

*Corresponding author (email: qigao@buaa.edu.cn)

decrease in accuracy. Numerous MART-based approaches have been developed to improve the efficiency and accuracy of 3D particle reconstruction. Additional details of MART-based algorithms were well analyzed by Scarano [2] and Gao et al. [7]. However, the ghost particle [8] and seeding density [9] issues are obstacles to achieving measurements with higher spatial resolutions by using MART-based methods.

Recently, researchers have realized that a few important features of particle intensity distributions have not yet been incorporated into tomographic reconstruction, namely the sparsity of the particle intensity distributions and the spherical intensity distributions of an individual particle [10]. The term "sparsity" is used to indicate that most voxels (more than 95%) in the measurement volume have zero intensity [11] and that only the volume that is occupied by tracer particles has non-zero intensity. Obviously, many researchers have been aware of this characteristic and have used it to optimize the MART and SMART. The multiplicative first guess (MFG) technique proposed by Worth and Nickels [12] and the multiplicative line-of-sight (MLOS) method by Atkinson and Soria [6] both use this characteristic to optimize the initial particle intensity distribution that is used for iteration. Both methods accelerate the convergence of the iterations and reduce the computational cost. The recently developed compressed sensing method [13] provides an effective tool for processing sparse and under-sampled signals and has been noticed probably practicable for tomographic reconstruction. Petra et al. [14,15] have conducted systematic investigations in this field, which have mainly focused on two topics: (1) Under what seeding density, the 3D particle distribution will be reconstructed accurately (without ghost particles)? (2) the conditions under which the l_0-norm can be replaced by the l_1-norm as an objective function in the optimization solver. The entire mathematical framework for applying compressed sensing to tomographic reconstruction has been established, and the next task is to apply the approach to actual experimental measurements.

A spherical particle intensity distribution is known *a priori* to indicate that the basic shape of the object to be reconstructed in Tomo-PIV is a small particle with uniform size. This feature is associated with the physical model of the particle projection weight function that is suggested in the MART and SMART, namely a cylinder-sphere intersection [16]. It results in a particle reconstruction with almost the same diameter as that of the image particles due to the diffraction of the tracer particles. This *a priori* knowledge was also discussed by Petra et al. [10], who proposed a Gaussian-type basis function to simulate the particle intensity distribution. The idea of using *a priori* particle intensity distribution knowledge has attracted greater attention recently. Multiple methods of implementing a spherical intensity distribution in tomographic reconstruction have been proposed, such as by using an optical transfer function [17], a point spread function [18], or a spatial filter [19].

Therefore, taking the sparsity and spherical intensity distribution features into account in Tomo-PIV reconstruction is a new trend to improve particle reconstruction algorithms. We propose a new technique involving dual-basis pursuit (DBP) and its derivative, dual-basis MART (DB-MART), to improve tomographic reconstruction. In Section 2, a brief introduction of the mathematical problem behind tomographic reconstruction is presented, and the concept of dual-basis is defined in detail. The 2D tests of the new techniques are discussed in Section 3.

2 Dual-basis techniques

2.1 The reconstruction problem

The physical problem of particle reconstruction in Tomo-PIV is to determine how to deduce an unknown 3D particle intensity distribution if the projections of those particles on multiple cameras are known. In mathematical terms, this process involves solving an inverse problem. If the unknown 3D particle intensity distribution is described by a 3D intensity matrix $\tilde{\boldsymbol{E}}$ with a size of $n_x \times n_y \times n_z$, it can be reshaped into a column matrix $\boldsymbol{E}_{n\times 1}$ with $n = n_x \times n_y \times n_z$. Here, the symbols with and without '~' represent the 3D matrix and its reshaped column matrix, respectively, unless the dimensions of the matrix are emphasized with subscripts. The projection function can be discretized as a transformation matrix $\boldsymbol{W}_{m\times n}$ (weighting matrix) that projects $\boldsymbol{E}$ onto its 2D intensity $\boldsymbol{I}_{m\times 1}$ on the camera. Here, m is the total number of pixels that record the projection of $\boldsymbol{E}$. The weighting matrix $\boldsymbol{W}_{m\times n}$ was calculated using the cylinder-sphere intersection model [16] in the current investigation. Therefore, the mathematics of particle reconstruction involves solving a system of linear equations:

$$\boldsymbol{WE} = \boldsymbol{I}, E_s \geqslant 0, (1 \leqslant s \leqslant n), \tag{1}$$

where s is the 1D index associated with the 3D indices of $\tilde{\boldsymbol{E}}$ at a location of (i_s, j_s, k_s).

Unfortunately, eq. (1) is a large-scale underdetermined linear system, since n is much larger than m. One method of making the problem solvable is to transform it into an optimization problem. Consequently, an objective function $f(\boldsymbol{E})$ is required to perform the optimization, and the problem becomes:

$$\min f(\boldsymbol{E}), \qquad \text{s.t.} \begin{cases} \boldsymbol{WE} = \boldsymbol{I}, \\ E_s \geqslant 0, (1 \leqslant s \leqslant n). \end{cases} \tag{2}$$

For the basic Tomo-PIV reconstruction technique, MART, the objective function is defined using information entropy:

$$f(\boldsymbol{E}) = -\sum_{s=1}^{n}(E_s / E^*)\ln(E_s / E^*), E^* = \sum_{s=1}^{n} E_s, \quad (3)$$

while its prototype, the algebraic reconstruction technique (ART), defines the objective function as l_2-norm of $\boldsymbol{E}$ [5]. All of the available MART-based methods that are used for Tomo-PIV reconstruction are based on the entropy criterion.

Recently, Sebastian et al. [20] suggested choosing l_1-norm of $\boldsymbol{E}$ to be an objective function and using the L1-regularized nonlinear least squares (L1-regularization) method to solve eq. (2). They showed that L1-regularization negligibly improved reconstructions with noise-free images. However, they noticed a slight quality improvement of the reconstructed volumes when L1-regularization was applied to a reconstruction with noisy images. This method will be evaluated and compared with the new methods in Section 3.

On the other hand, eq. (2) has four features (**B1–B4**) that constrain the solution [10,21].

B1: the linear equation system is a very large-scale underdetermined system.

B2: $\boldsymbol{E}$ is a sparse column matrix.

B3: $\boldsymbol{E}$, in its 3D format ($\tilde{\boldsymbol{E}}$), has a local pattern of solution, which is the basic intensity distribution of a particle.

B4: the elements of $\boldsymbol{E}$ are all non-negative, so $E_s \geq 0$.

Petra et al. [10] noted that the current reconstruction techniques (the ART-based and MART-based methods) are limited since they do not apply **B3**. To involve **B3** in particle reconstruction, manual intervention is required to restrict and guide the iteration. Using a template of particle intensity distribution for solving $\boldsymbol{E}$ is an ingenious idea and could be performed by using a Gaussian-type basis function [10], and then the optimization problem becomes

$$\min f(\boldsymbol{E}'), \qquad \text{s.t.}\begin{cases}\boldsymbol{W}\boldsymbol{M}\boldsymbol{E}' = \boldsymbol{I}, \\ \boldsymbol{E}'_s \geqslant 0, (1 \leqslant s \leqslant n),\end{cases} \quad (4)$$

where $\boldsymbol{M}_{n\times n}$ is the basis function matrix of the particle template, and $\boldsymbol{E}'_{n\times 1}$ is the projection coefficient that satisfies

$$\boldsymbol{E} = \boldsymbol{M}\boldsymbol{E}'. \quad (5)$$

In a template-based optimization method, the basis function can not only restrict the solution to having a highly locally isotropic intensity distribution, but also accelerate the iteration towards reaching a sparse solution. However, designing an appropriate set for a template basis (TB) is not an easy task. Theoretically, a set of linearly independent basis can span a convex space R^n without constraint **B4**. When $\boldsymbol{E}$, $\boldsymbol{M}$, and $\boldsymbol{E}'$ are all non-negative, the basis must be orthogonal. Unfortunately, it seems that only one basis function matrix $\boldsymbol{M}$ meets the requirement of orthogonality, namely an $\boldsymbol{M}$ that is proportional to the identity matrix, which does not include any *a priori* knowledge of the particle intensity distribution. On the contrary, a residual is generated from eq. (5), if a Gaussian-type basis function (rather than an orthogonal one) is used for $\boldsymbol{M}$. Therefore, we introduced a dual-basis into eq. (5) to overcome the residual issue.

2.2 Dual-basis technique

In Tomo-PIV reconstruction, a Gaussian-type TB is a superior candidate for $\boldsymbol{M}$, but it is not easy to make such bases orthogonal, which means that they can only span sub-spaces of the solution space if $\boldsymbol{E} \geqslant 0$. In other words, a set of linearly independent TB could not reconstruct a 3D particle field with sub-voxel accuracy. Consequently, there is a residual $\boldsymbol{\varepsilon}$, which turns eq. (5) into

$$\boldsymbol{E} = \boldsymbol{M}_1\boldsymbol{E}'_1 + \boldsymbol{\varepsilon}, \quad (6)$$

where $\boldsymbol{M}_1$ and $\boldsymbol{E}'_1$ are the Gaussian-type particle TB and its corresponding coefficient column matrix, respectively. The residual is $\boldsymbol{\varepsilon}_{n\times 1}$. Furthermore, $\boldsymbol{\varepsilon}$ can also be decomposed into a linear combination of an orthogonal standard basis $\boldsymbol{M}_2$ with coefficient $\boldsymbol{E}'_2 \geqslant 0$, resulting in:

$$\boldsymbol{E} = \boldsymbol{M}_1\boldsymbol{E}'_1 + \boldsymbol{M}_2\boldsymbol{E}'_2. \quad (7)$$

We define $\boldsymbol{M}_1$ as the TB and $\boldsymbol{M}_2$ as the correcting basis (CB). Here, a Gaussian basis function is used for the TB. To describe the TB, $\tilde{\boldsymbol{M}}_1^{(s)}$ is defined as the 3D version of $\boldsymbol{M}_1^{(s)}$, the s-th column of $\boldsymbol{M}_1$. Thus,

$$\tilde{\boldsymbol{M}}_{1,ijk}^{(s)} = \begin{cases} C_1 \exp\left(-\dfrac{\| \boldsymbol{p} - \boldsymbol{p}_s \|_2^2}{2\sigma^2}\right), \text{if } \| \boldsymbol{p} - \boldsymbol{p}_s \|_2 \leqslant D/2, \\ 0, \text{if } \| \boldsymbol{p} - \boldsymbol{p}_s \|_2 > D/2, \end{cases} \quad (8)$$

where the constant C_1 is the maximum intensity of the Gaussian basis, σ is the standard deviation of the Gaussian distribution, $\boldsymbol{p} = (i, j, k)$, $\boldsymbol{p}_s = (i_s, j_s, k_s)$, and D is the diameter of the particle template. Practically, the parameters C_1 and σ can be acquired from an averaged 2D particle intensity distribution obtained from projections of individual particles on images. To guarantee including at least 95% of the intensity of a particle, D can be set to 4σ. Similarly, the s-th column of $\boldsymbol{M}_2$ is defined as:

$$\tilde{\boldsymbol{M}}_2^{(s)} = \begin{cases} C_2, & \text{if } \boldsymbol{p} = \boldsymbol{p}_s, \\ 0, & \text{if } \boldsymbol{p} \neq \boldsymbol{p}_s, \end{cases} \quad (9)$$

where C_2 is a constant intensity of the CB, which could normally be set equal to C_1. Therefore, $\boldsymbol{M}_2$ is proportional to the identity matrix. The orthogonality of $\boldsymbol{M}_2$ makes the combination of $\boldsymbol{M}_1$ and $\boldsymbol{M}_2$ span the full solution space of eq. (5). Figure 1 explains the roles of the TB and CB in reconstructing a particle (in a 1D example). The TB is a symmetric model of the intensity distribution, while the CB can

help shift the intensity peak to enable sub-voxel accuracy at the particle center. Therefore, any particle intensity distribution can be reconstructed with a combination of the TB and CB, as in eq. (7). Eventually, eq. (2) becomes

$$\min f(\boldsymbol{E}_1', \boldsymbol{E}_2'), \quad \text{s.t.} \begin{cases} \boldsymbol{W}(\boldsymbol{M}_1\boldsymbol{E}_1' + \boldsymbol{M}_2\boldsymbol{E}_2') = \boldsymbol{I}, \\ E_{1,s}, E_{2,s} \geqslant 0, (1 \leqslant s \leqslant n). \end{cases} \tag{10}$$

Similar to eq. (2), different objective functions $f(\boldsymbol{E}_1', \boldsymbol{E}_2')$ will lead to different results. We propose two methods with different objective functions in the following two sections.

2.3 Dual-basis pursuit (DBP)

To solve an underdetermined linear system with sparse solutions, which is a classical NP-hard problem, mathematicians have developed various tools, such as matching pursuit [22], basis pursuit [23], and compressed sensing [13]. These techniques are well accepted and have applications in various fields, including in fluid mechanics.

The technique of compressed sensing normally utilizes l_q-norm ($0 \leqslant q \leqslant 1$) as the objective function, which has strong physical meaning in image processing when $E_s \geqslant 0$. The summation of $\boldsymbol{E}$ is represented by l_1-norm, which has been studied by Sebastian et al. [20] and is defined as L1-regularization, while l_0-norm indicates the total number of positive elements of $\boldsymbol{E}$. In the L1-regularization method, eq. (2) is solved based on the objective function, l_1-norm of $\boldsymbol{E}$. Petra and Schröder [15] constructed a theoretical framework to apply compressed sensing to Tomo-PIV reconstruction. Cornic et al. [24] first investigated the performance of the compressive sampling matching pursuit (CoSaMP) in tomographic reconstruction. Combined with a local maxima detection algorithm, the CoSaMP approach clearly outperformed classical SMART.

In our dual-basis pursuit (DBP), l_1-norm of $\boldsymbol{E}_2'$ is defined as the objective function. Minimizing $\| \boldsymbol{E}_2' \|_1$ means maximizing the correlation between the real intensity distribution and the TB, which makes the objective function bounded. Therefore, the optimization problem (eq. (10)) becomes

$$\min \| \boldsymbol{E}_2' \|_1, \quad \text{s.t.} \begin{cases} \boldsymbol{W}(\boldsymbol{M}_1\boldsymbol{E}_1' + \boldsymbol{M}_2\boldsymbol{E}_2') = \boldsymbol{I}, \\ \boldsymbol{E}_{1,s}', \boldsymbol{E}_{2,s}' \geqslant 0, (1 \leqslant s \leqslant n). \end{cases} \tag{11}$$

There are other two potential objective functions that are similar to $\| \boldsymbol{E}_2' \|_1$, namely $\| \boldsymbol{E}_1' \|_1$ and $\| \boldsymbol{E}_1' \|_1 + \| \boldsymbol{E}_2' \|_1$. When $\| \boldsymbol{E}_1' \|_1$ is minimized, the TB will be disabled, since the CB $\boldsymbol{M}_2$ is orthogonal and is able to solely span the full solution space. Thus, the algorithm reduces to L1-regularization. When $\| \boldsymbol{E}_1' \|_1 + \| \boldsymbol{E}_2' \|_1$ acts as an objective function, both the TB and CB are counted with the same weight. The weights of the CB and TB could be modified in the objective function by changing C_1 and C_2 in eqs. (8) and (9), respectively. Numerical simulations have been performed to test the difference between objective functions $\| \boldsymbol{E}_2' \|_1$ and $\| \boldsymbol{E}_1' \|_1 + \| \boldsymbol{E}_2' \|_1$, and minor differences have been observed. Therefore, to lower the computational cost, $\| \boldsymbol{E}_2' \|_1$ was chosen as the objective function of DBP in this study. Since both the constraints and the objective function are linear in eq. (11), a linear program algorithm could be used to solve.

2.4 Dual-basis MART

As mentioned in Section 2.1, the MART uses entropy in the objective function to solve the optimization problem of eq. (2). Following the same idea, we used the MART to solve eq. (10), which can be rewritten as:

$$\min f(\boldsymbol{E}'), \quad \text{s.t.} \begin{cases} \boldsymbol{B}\boldsymbol{E}' = \boldsymbol{I}, \\ \boldsymbol{E}'_s \geqslant 0, (1 \leqslant s \leqslant 2n), \end{cases} \tag{12}$$

where $\boldsymbol{B} = \boldsymbol{W}[\boldsymbol{M}_1, \boldsymbol{M}_2]$, $\boldsymbol{E}' = \begin{pmatrix} \boldsymbol{E}_1' \\ \boldsymbol{E}_2' \end{pmatrix}$, and $f(\boldsymbol{E}')$ is defined as the entropy of $\boldsymbol{E}'$, which is similar to its definition in eq. (3). Thus, eq. (12) has the same format as eq. (2), which means that the MART iteration algorithm could be adopted to reconstruct the particle intensity field. We named the new algorithm DB-MART. Its iterative formula is as follows.

DB-MART:

$$\begin{aligned} &E'(X_j, Y_j, Z_j)^{k+1} = CF \cdot E'(X_j, Y_j, Z_j)^k, \\ &CF = [I(x_i, y_i) / \sum_{j \in \Phi_i} b_{ij} E'(X_j, Y_j, Z_j)^k]^{\mu b_{ij}}, \end{aligned} \tag{13}$$

where CF is a correction factor, (X_j, Y_j, Z_j) are the coordinates of the j-th voxel, (x_i, y_i) are the coordinates of the i-th

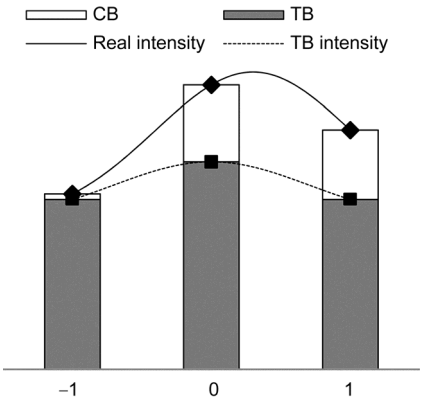

Figure 1 Schematic of TB and CB (1D). Combination of TB and CB achieves sub-grid intensity distribution.

pixel, b_{ij} is an element of $\boldsymbol{B}$, μ is a scalar relaxation parameter, Φ_i is the set of all voxels that can affect the i-th pixel, and k represents the k-th iteration. The initial value of the DB-MART can be estimated using the MFG or MLOS technique with the following formulas.

MFG:

$$E_{0,j}^{'} = \left[\prod_{k=1}^{N_c} \left(\sum_{i \in \Phi_j^k} b_{ij} I_i \right) \right]^{1/N_c}, \tag{14}$$

MLOS:

$$\boldsymbol{E}_{0,j}^{'} \ \boldsymbol{E}_{0,j}^{'} = \left[\prod_{i \in \Phi_j} \left(I_i^{b_{ij}} \right) \right]^{1/N_c}, \tag{15}$$

where $\boldsymbol{E}_0^{'}$ is the initial value of $\boldsymbol{E}^{'}$, $\boldsymbol{E}_{0,j}^{'}$ is the j-th voxel of $\boldsymbol{E}_0^{'}$, N_c is the number of cameras, $\boldsymbol{\Phi}_j^k$ is the set of all pixels on the k-th camera that are affected by the j-th voxel, and Φ_j is the set of all pixels that are affected by the j-th voxel on all cameras.

To facilitate following of the procedures of the new methods, a flow chart is provided in Figure 2.

3 Numerical assessment

The performances of the DBP and DB-MART were assessed via a typical 2D numerical test of Tomo-PIV reconstruction for algorithm study, which was the same as the 2D test used by Elsinga et al. [1] and Discetti et al. [19]. Unless stated otherwise, synthetic particles with sizes of 3×3 voxels were randomly generated and distributed in a 2D test domain with a grid size of 1000×200. The synthetic particles had a Gaussian intensity distribution with a maximum intensity of 200 counts and a standard deviation of σ_s = 0.75 pixels, which is 1/4 of the particle diameter [25]. One-dimensional projections of the particles on four virtual cameras were synthesized. The four cameras were aligned at viewing angles in increments of 20°, resulting in a total viewing range of 60° (Figure 3). The TB defined by eq. (8) was used with C_1 = 1, $\sigma = \sigma_s$ = 0.75, and $D = 4\sigma$, while C_2 was set equal to C_1 for the CB.

Different algorithms were tested for comparison. All of the settings of the tested methods are summarized as follows: In the MART, the standard settings were used with five iteration steps and relaxation factor = 1; in the DB-MART, the same settings were used as in the MART; and both the DBP and L1-regularization were implemented in the MATLAB environment using the optimization function *linprog* with the algorithm of a "large-scale interior point." The iteration was exit when the residual between the original and new projections of the reconstructed volume decreased to below a critical value of 0.1.

Figure 4 shows the test results for the normalized correlation coefficients Q [1] of the exact and reconstructed

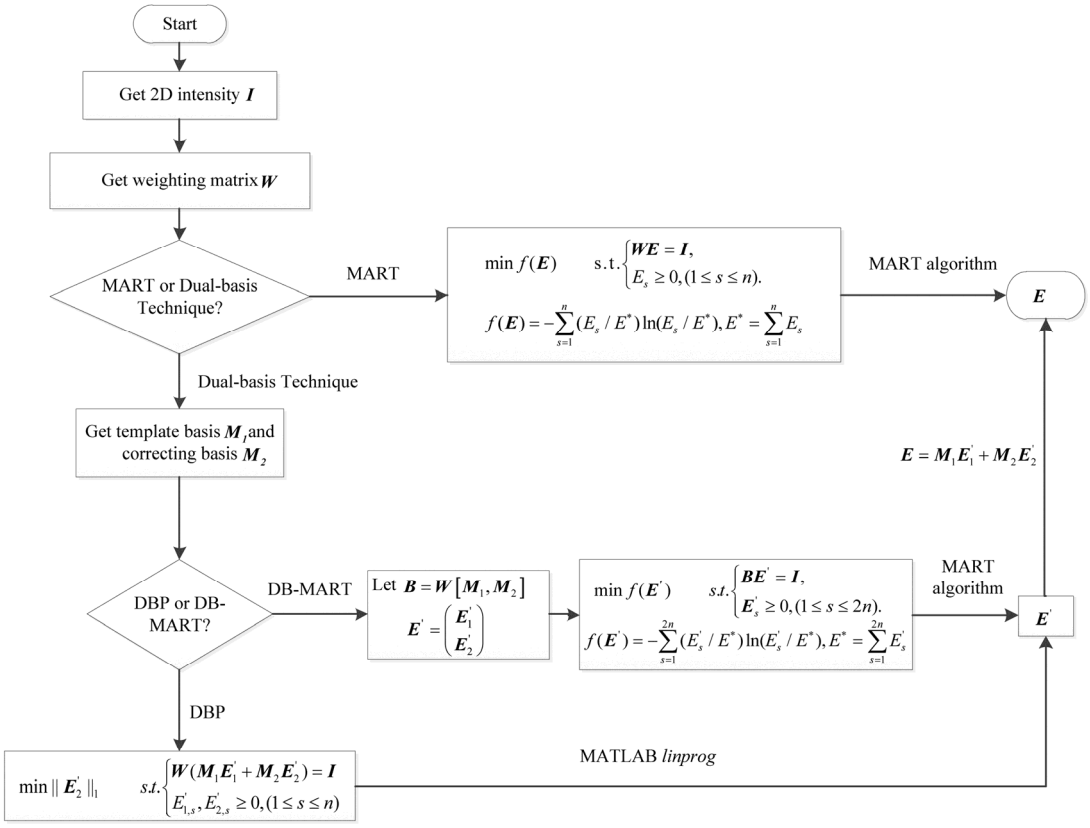

Figure 2 Flow chart of reconstruction methods.

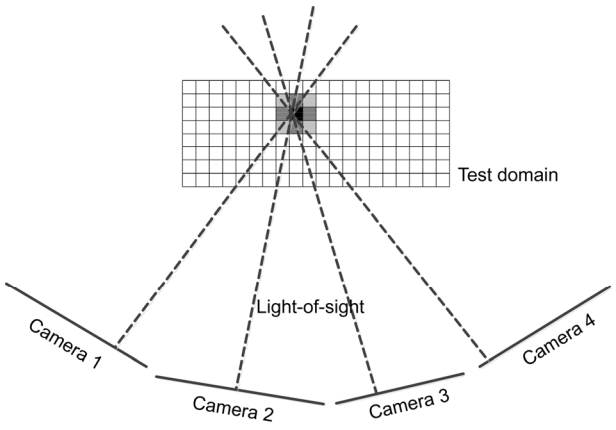

Figure 3 Schematic of arrangement of cameras.

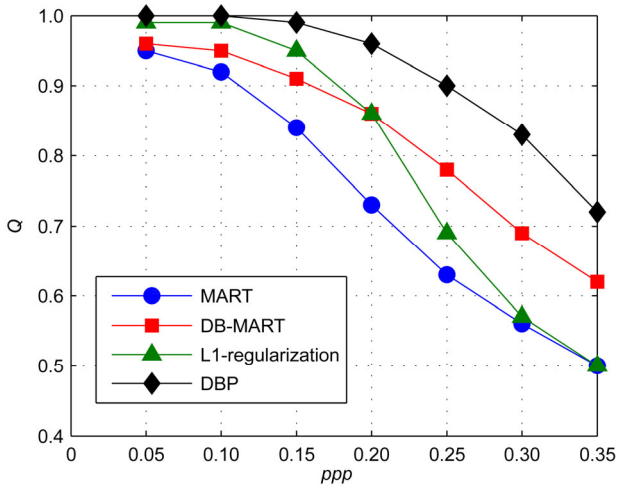

Figure 4 Comparison of quality factors Q for different reconstruction techniques while varying seeding density, *ppp*.

intensity distributions with various seeding densities (*ppp*, particles per pixel). Significant improvement in the particle reconstruction was achieved by using the dual-basis pursuit technique. For a particle field with $ppp < 0.15$, the DBP technique could perfectly recover the particle distribution with $Q > 0.99$, while for $ppp > 0.3$, Q remains above 0.8, although the particle field is too dense to be reconstructed well using any other algorithm. The L1-regularization method only shows high Q values at small seeding densities ($ppp < 0.1$), and it rapidly decreases with increasing seeding density. The L1-regularization Q values are even lower than those of the DB-MART algorithm for $ppp > 0.2$. The difference between the DBP and L1-regularization indicates the importance of the TB, which is also verified by comparing the performance of the DB-MART with that of the MART. With the addition of the TB, the DB-MART shows higher Q values than does the MART, especially for highly seeded fields. The improvements in the DBP and DB-MART suggest that the sparsity that was discussed in Section 1 (the use of different objective functions) is another important behavior that can be used to advance current particle reconstruction approaches.

Figure 5 provides the probability density functions (PDF) of the peak intensities of ghost and actual particles in the test case of $ppp = 0.15$. The PDFs of the actual particles and ghost particles in the DBP have no overlap, which suggests that the ghost particles can be further removed from the reconstructed particles. Furthermore, the intensity of the PDF peak of the actual particles in the DBP result is close to the maximum intensity of the synthetic particles, 200 counts,

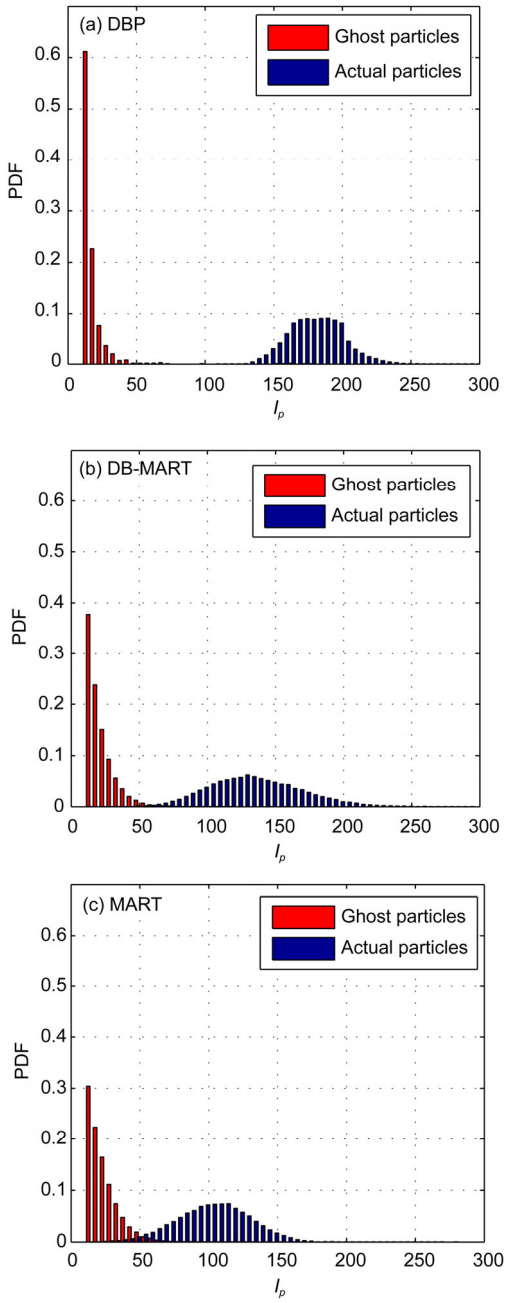

Figure 5 PDFs of particle peak intensities for ghost and actual particles in test case with $ppp = 0.15$ and use of (a) DBP, (b) DB-MART, and (c) MART.

while for the other two algorithms, the peak intensities are smaller. Therefore, the ghost particles are very weak in the DBP method (high PDF for small intensity) which take less intensities from the reconstructed actual particles. On the other hand, the number of ghost particles in the DBP is less than the numbers in the other two techniques. Only 4% of the total number of reconstructed particles are ghost particles, while the ratio increases to about 54% and 65% with use of the DB-MART and MART algorithms, respectively.

Table 1 shows the memory usages and computation times required for all of the 2D simulation tests that were conducted with the four different reconstruction methods. It shows that the DBP has the fastest processing speed but also the greatest memory requirement. Further tests showed that the memory requirement increased rapidly as the reconstruction volume increased.

Although the DBP performed well, it cannot be used in 3D applications at the moment due to computational memory limitations. Fortunately, the DB-MART has the potential to be adopted for 3D applications. Thus, further tests will primarily focus on evaluating the DB-MART. However, we only focus on 2D tests in the current work.

3.1 Effect of the TB standard deviation on the DB-MART

Tracer particles are generally very small. Their projection images on cameras are mainly Airy spots due to diffraction, which can be approximated as Gaussian intensity distributions [25]. Normally, the sizes and shapes of particle images can be considered uniform; specifically, the diameters and standard deviations of the intensity distributions of particle images are assumed to be uniform. Furthermore, it is assumed that reconstructed 3D particles have the same intensity distribution standard deviations as those of the particle images. Thus, the sizes and standard deviations of the 3D particles that were used to generate the TB for the DB-MART were statistically obtained from the 2D particle images. When standard deviation mismatching exists between the TB and the real 3D particle, it affects the particle reconstruction accuracy. Therefore, a parametric study of the robustness of the standard deviation was conducted. For a synthetic image particle standard deviation σ_s varying from 0.55 to 0.95 (the diameter of the synthetic image particles was $4\sigma_s$) and a TB standard deviation remaining at 0.75, Figure 6 shows the effect of the TB standard deviation on the quality factor Q. It suggests that a smaller TB standard deviation is better for reconstructing particles with larger σ_s values. Although the variation of σ_s/σ has a range of $\pm 30\%$, the change in Q remains under 5%. Therefore, the TB standard deviation can be directly set to 0.75 without statistical evaluation of σ_s from 2D particle images.

Table 1 Memory usages and computation times required by different methods

	MART	DB-MART	L1-regularization	DBP
Time (s)	39.7	70.6	67.4	10.1
Memory (GB)	2.19	2.49	5.80	5.84

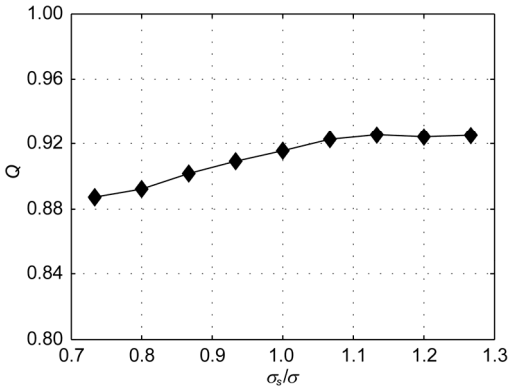

Figure 6 Effect of standard deviation. Standard deviation of synthetic particles σ_s varies from 0.55 to 0.95, while that of TB remains 0.75. Here, $ppp = 0.15$, $\mu = 1$, and five iterations were used.

3.2 Effect of noise in the DB-MART

In this section, two types of noise in the particle reconstruction in the DB-MART are discussed, namely, the random background noise in the particle images and the noise in the images due to additional particles located outside of the reconstruction volume [1]. Figure 7 shows the effect of random noise (white noise) on the reconstruction. The noise level is given as a percentage of the peak particle intensity. Figure 8 shows the effect of additional particles on the reconstruction, where the added particle rate is the ratio of additional particles to existing particles in the measurement domain. Both types of noise cause Q to linearly decrease. Between these two types of noise, it seems that random noise in images has a larger influence on the reconstruction. Q decreases by about 20% when the random noise increases to 50%. When the additional particle rate increases to 50%, about 1/3 of the particle images are unmatched between the cameras, which is a fairly high disturbance to the particle

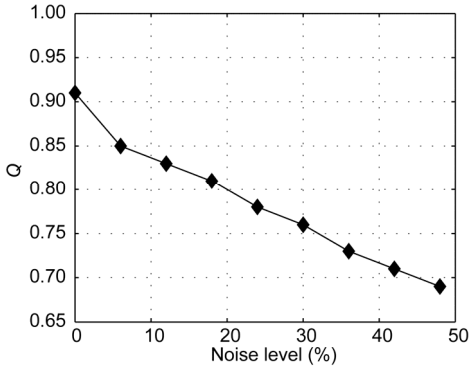

Figure 7 Effect of random noise on reconstruction.

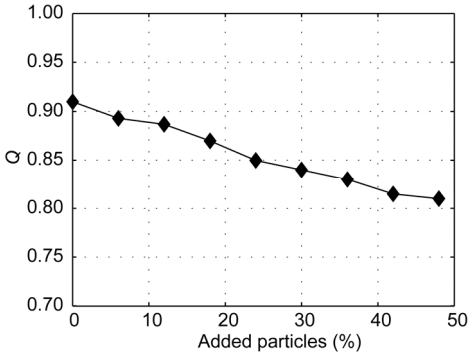

Figure 8 Effect of additional particles on reconstruction.

reconstruction. However, Q decreases by only about 10%. The results show that the DB-MART is reliable even with measurement noise.

4 Conclusion

Tomographic particle reconstruction was discussed in the current work. Several approaches to solving the underdetermined system of linear equations were reviewed. As a good way of reconstructing particles using an optimization method, the idea of basis pursuit was applied. Thus, a dual-basis pursuit technique was proposed to perform tomographic particle reconstruction. The new method incorporates two important particle distribution features into the tomographic reconstruction, namely, particle distribution sparsity and the spherical intensity distribution of a particle. A Gaussian intensity distribution template combined with a correcting template proportional to the identity matrix was designed as *a priori* knowledge to reconstruct a particle intensity field with sub-voxel accuracy. The l_1-norm criterion was used as the objective function to cause particle field sparsity in the DBP.

The 2D numerical tests showed that the DBP technique was superior to the other particle reconstruction approaches. It could completely recover particle fields with $ppp < 0.15$ and maintain a quality factor Q of above 0.8 for ppp up to 0.30. Unfortunately, the DBP method is difficult to utilize in 3D applications due to its unaffordable memory usage requirements.

Therefore, a dual-basis MART was designed that had better performance than that of the traditional MART and can potentially be utilized in 3D applications. Further study of the DB-MART performance with noise was conducted. The parametric DB-MART study showed that it was robust and exhibited stable performance with variations in the standard deviation of the TB, random noise, and additional particle noise in the images.

As new tomographic reconstruction methods, the DBP and DB-MART need to be extended to 3D measurement applications.

This work was supported by the National Natural Science Foundation of China (Grant Nos. 11472030, 11327202 and 11490552)

1 Elsinga G E, Scarano F, Wieneke B, et al. Tomographic particle image velocimetry. Exp Fluids, 2006, 41: 933–947
2 Scarano F. Tomographic PIV: Principles and practice. Meas Sci Tech, 2013, 24: 012001
3 Herman G T, Lent A. Iterative reconstruction algorithms. Comput Biol Med, 1976, 6: 273–294
4 Natterer F. Numerical methods in tomography. Acta Numer, 1999, 8: 107–141
5 Gordon R, Bender R, Herman G T. Algebraic reconstruction techniques (ART) for three-dimensional electron microscopy and X-ray photography. J Theor Biol, 1970, 29: 471–481
6 Atkinson C, Soria J. An efficient simultaneous reconstruction technique for tomographic particle image velocimetry. Exp Fluids, 2009, 47: 553–568
7 Gao Q, Wang H P, Shen G X. Review on development of volumetric particle image velocimetry. Chin Sci Bull, 2013, 58: 4541–4556
8 Elsinga G, Westerweel J, Scarano F, et al. On the velocity of ghost particles and the bias errors in Tomographic-PIV. Exp Fluids, 2011, 50: 825–838
9 Michaelis D, Novara M, Scarano F, et al. Comparison of volume reconstruction techniques at different particle densities. In: 15th International Symposium on Applications of Laser Techniques to Fluid Mechanics, Lisbon, Portugal, 2010
10 Petra S, Schnörr C, Schröder A, et al. Tomographic image reconstruction in experimental fluid dynamics: Synopsis and problems. In: Ion S, Marinoschi G, Popa C, eds. Mathematical Modelling of Environmental and Life Sciences Problems, Bucuresti: Ed. Acad. Romane, 2007. 1–21
11 Westerweel J, Elsinga G E, Adrian R J. Particle image velocimetry for complex and turbulent flows. Annu Rev Fluid Mech, 2013, 45: 409–436
12 Worth N A, Nickels T B. Acceleration of Tomo-PIV by estimating the initial volume intensity distribution. Exp Fluids, 2008, 45: 847-856
13 Donoho D L. Compressed sensing. IEEE T Inform Theory, 2006, 52: 1289–1306
14 Petra S, Schnörr C. TomoPIV meets compressed sensing. In: ICNAAM 2010: International Conference of Numerical Analysis and Applied Mathematics, Athens, Greece, 2010
15 Petra S, Schröder A, Schnörr C. 3D tomography from few projections in experimental fluid dynamics. Imag Meas Meth Flow Anal, 2009, 63–72,
16 Lamarche F, Leroy C. Evaluation of the volume of intersection of a sphere with a cylinder by elliptic integrals. Comput Phys Commun, 1990, 59: 359–369
17 Schanz D, Gesemann S, Schröder A, et al. Non-uniform optical transfer functions in particle imaging: calibration and application to tomographic reconstruction. Meas Sci Tech, 2013, 24: 024009
18 Champagnat F, Cornic P, Cheminet A, et al. Tomographic PIV: particles vs blobs. In: 10th International Symposium on Particle Image Velocimetry, Delft, The Netherlands, 2013
19 Discetti S, Natale A, Astarita T. Spatial filtering improved tomographic PIV. Exp Fluids, 2013, 54: 1–13
20 Sebastian G, Daniel S, Andreas S, et al. Recasting Tomo-PIV reconstruction as constrained and L1-regularized non-linear least squares problem. In: 15th International Symposium on Applications of Laser Techniques to Fluid Mechanics, Lisbon, Portugal, 2010
21 Barbu I, Herzet C, Memin E. Sparse models and pursuit algorithms for piv tomography. In: Forum on Recent Developments in Volume Reconstruction Techniques Applied to 3D Fluid and Solid Mechanics, Futuroscope Chasseneuil, France, 2011
22 Mallat S G, Zhang Z. Matching pursuits with time-frequency dictionaries. IEEE T Signal Proces, 1993, 41: 3397–3415
23 Chen S S, Donoho D L, Saunders M A. Atomic decomposition by basis pursuit. SIAM J Sci Comput, 1998, 20: 33–61
24 Cornic P, Champagnat F, Cheminet A, et al. Computationally efficient sparse algorithms for tomographic PIV Reconstruction. In: 10th International Symposium on Particle Image Velocimetry, Delft, The Netherlands, 2013
25 Adrian R J, Westerweel J. Particle Image Velocimetry. 2nd ed. London: Cambridge University Press, 2010